Research Square

Preprints are preliminary reports that have not undergone peer review.
They should not be considered conclusive, used to inform clinical practice,
or referenced by the media as validated information.

Species-dependent opioid receptor pharmacology in dogs revealed by binding, signaling, and structural analysis

Elena K. Gerdes
Ludwig-Maximilians-Universität München
Christian Zenner
Ludwig-Maximilians-Universität München
Sarah Koutnik-Abele
University of Würzburg
Hermann Ammer
h.ammer@lmu.de

Ludwig-Maximilians-Universität München

Article

Keywords: opioid receptors, species differences, ligand binding, ERK1/2 signaling, comparative pharmacology

Posted Date: October 5th, 2026

DOI: https://doi.org/10.21203/rs.3.rs-10851767/v1

License: This work is licensed under a Creative Commons Attribution 4.0 International License. Read Full License

Additional Declarations: No competing interests reported.

Abstract

Opioid analgesics show variable clinical efficacy across species, whose underlying mechanisms remain insufficiently characterized. Besides pharmacokinetic factors, the present study investigates whether differences in opioid receptor structure and function might contribute to canine-specific opioid pharmacology. Here, we cloned canine μ- (cMOR) and k-opioid receptors (cKOR), expressed them in HEK293 cells, and evaluated ligand binding and ERK1/2 signaling for clinically relevant opioids, comparing results with rat MOR and human KOR. Molecular docking identified conserved and species-specific ligand-receptor interactions. Buprenorphine exhibited high affinity but reduced signaling at canine receptors; morphine showed enhanced μ-selectivity with near-maximal efficacy; butorphanol acted as a full agonist at cKOR but a weak partial agonist at cMOR. These findings demonstrate that opioid receptor sequence variation contributes to species-dependent pharmacodynamics, providing molecular insights relevant to veterinary opioid use and highlighting the value of integrating experimental and computational approaches in comparative pharmacology.

Introduction

Opioids are widely used for analgesia and sedation in veterinary medicine. However, dosing regimens and clinical responses differ markedly among species [1]. Differences in drug metabolism and elimination contribute to this variability, but pharmacokinetic differences do not fully account for species-dependent drug effects [2]. Pharmacodynamic differences at the receptor level may therefore represent an additional determinant of interspecies variability [3]. Detailed characterization of opioid receptor pharmacology in target species is consequently important for understanding and predicting opioid responses in veterinary patients.

Opioid receptors are G protein-coupled receptors (GPCRs) that mediate important components of nociception at the spinal and supraspinal levels [4]. The three classical opioid receptor types are the μ-opioid receptor (MOR), k-opioid receptor (KOR) and δ-opioid receptor (DOR). Whereas MOR activation controls somatic pain mechanisms, KOR activation contributes to spinal and visceral pain pathways [5, 6]. The functional contribution of DOR signaling is more context-dependent and is not yet fully understood [7].

Ligand binding induces conformational changes in opioid receptors that regulate G protein-dependent and G protein-independent signaling pathways including extracellular signal-regulated kinase 1/2 (ERK1/2) [8, 9]. The magnitude of downstream signaling is commonly used as a cellular measure of ligand efficacy [10], whereas receptor affinity and selectivity can be characterized by radioligand binding [11]. These pharmacological properties contribute to the conventional classification of opioids as full, partial, or mixed agonists. However, it is important to note that antinociceptive efficacy of opioids is also influenced by factors such as receptor density, receptor coupling efficiency, and the cellular signaling environment [12].

Clinically used opioids differ substantially in their pharmacological profiles. In dogs, fentanyl is a potent analgesic [13], whereas morphine is less effective and already induces gastrointestinal adverse effects and histamine release at therapeutic concentrations [14]. Buprenorphine is a high-affinity opioid with partial agonist properties and is used in dogs for peri-operative and post-operative analgesia and sedation [15]. Butorphanol is commonly described as a mixed agonist–antagonist, with prominent KOR activity and more limited MOR activity [16, 17]. The extent to which these pharmacological profiles are preserved at the molecular level in canine opioid receptors remains insufficiently characterized.

In this study, we characterized the binding and signaling properties of clinically relevant opioid analgesics at cloned canine MOR and KOR, comparing them with rat MOR and human KOR reference receptors. Additionally, we employed molecular docking to identify conserved and ligand-specific receptor contacts that may underlie species-dependent pharmacological differences, thereby providing molecular insights into the basis of canine-specific opioid responses.

Results

Cloning and sequence analysis of canine opioid receptors

RT-PCR cloning yielded cDNA fragments of 1,143 bp for canine *OPRK1* and 1,206 bp for canine *OPRM1*. The sequences were deposited in GenBank as cKOR1 (KP676947.1) and cMOR1 (KP676946.1). Canine *OPRK1* comprises three exons on chromosome 29, whereas canine *OPRM1* comprises four exons on chromosome 1 (Fig. 1). The predicted proteins showed approximately 93% sequence identity between cKOR and hKOR and approximately 94% identity between cMOR and rMOR. Sequence differences occurred mainly in the N- and C-terminal regions, whereas the transmembrane domains forming the orthosteric pharmacophore were largely conserved. Only three amino-acid differences were identified within transmembrane domains (TM) V and VI of cKOR (hV215 → cI215; hV297 → cI297; hV298 → cI298), and one substitution was identified in extracellular loop II of cMOR (rQ212 → cH215) compared to reference receptors (Fig. 2).

Opioid binding affinity at canine and reference receptors

Determination of pK_i values for the opioid analgesics first required measurement of the affinity of the radioligand [^{3}H]naloxone at each receptor. Besides the expected differences between μ- and k-opioid receptors, naloxone affinity also varied between canine and reference μ- and k-receptors (K_d = 0.25 ± 0.1 nM at cMOR and 0.56 ± 0.1 nM at rMOR; 1.26 ± 0.2 nM at cKOR, 2.61 ± 0.3 nM at hKOR).

Using receptor-specific [^{3}H]naloxone affinities, exact pK_i values for the opioid analgesics were determined by heterologous displacement experiments. The μ-selective, synthetic anilinopiperidine derivative fentanyl showed no species differences in MOR binding, with similarly high affinity at cMOR and rMOR (pK_i = 7.81 ± 0.1). Binding to cKOR and hKOR (pK_i > 5) was negligible. In contrast, morphinan derived opioids exhibited ligand- and receptor-specific differences in affinity. The partial μ-agonist buprenorphine showed even higher affinities for canine receptors than for the reference receptors (pK_i = 10.98 ± 0.1 at cMOR;

10.59 ± 0.1 at rMOR; 10.22 ± 0.1 at cKOR; 9.72 ± 0.04 at hKOR). The prototypical μ-agonist morphine exhibits even higher μ-selectivity due to an increased affinity at cMOR compared to rMOR (8.63 ± 0.1 versus 8.06 ± 0.1) and lower affinity at cKOR compared to hKOR (7.04 ± 0.1 versus 7.30 ± 0.1). The mixed agonist butorphanol showed overall comparable affinity at cMOR, cKOR and hKOR (9.55 ± 0.1, 9.46 ± 0.1 and 9.42 ± 0.1, respectively), with a somewhat lower affinity at rMOR (9.16 ± 0.1). Thus, receptor sequence differences were associated with ligand-dependent changes in the binding affinity and receptor selectivity of opioid analgesics with a morphinan structure. A summary of all binding data is presented in Fig. 3.

Docking identifies conserved and ligand-specific receptor contacts

Docking studies using AlphaFold3-derived receptor models and Boltz-2, a model that predicts small molecule-protein binding affinity, confirmed that all opioids investigated occupied a conserved orthosteric pocket in all receptors. Conserved interactions involved residues in TM III, including Asp138/138/150/147, Tyr139/139/151/148, Met142/142/154/151 and Val230/230/239/236 in hKOR/cKOR/cMOR/rMOR, respectively (Table 1).

Table 1

Opioid ligand binding sites predicted by molecular docking. Conserved contact sites (blue), and ligand characteristic contact sites (red) are highlighted. NT terminus; TM, transmembrane domain; ECL, extracellular loop. Contact sites were evaluated using a negative overlap cutoff of − 0.4 Å.

	Fentanyl		Buprenorphine				Morphine				Butorphanol			
	cMOR	rMOR	hKOR	cKOR	cMOR	rMOR	hKOR	cKOR	cMOR	rMOR	hKOR	cKOR	cMOR	rM
NT				Ser27	Ser31	Ser28								
				Gly28	Gly30	Gly27								
	Trp32			Trp29	Trp32	Trp29								
TM II			Val108								Val108			
			Gln115											
	Gln127	Gln124												
ECL I	Trp136	Trp133												
TM III	Val146													
	Asp150	Asp147	Asp138	Asp138	Asp150	Asp147	Asp138	Asp138	Asp150	Asp147	Asp138	Asp138	Asp150	Asp
	Tyr151	Tyr148	Tyr139	Tyr139	Tyr151	Tyr148	Tyr139	Tyr139	Tyr151	Tyr148	Tyr139	Tyr139	Tyr151	Tyr
	Met154	Met151	Met142	Met142	Met154	Met151	Met142	Met142	Met154	Met151	Met142	Met142	Met154	Met
ECL II		Cys217												
TM V	Val239	Val236	Val230	Val230	Val239	Val236	Val230	Val230	Val239	Val236	Val230	Val230	Val239	Val
TM VI	Trp296	Trp293	Trp287	Trp287	Trp296	Trp293		Trp287	Trp296		Trp287	Trp287	Trp296	Trp
				His291				His291				His291		
	Ile299	Ile296	Ile294	Ile294	Ile299	Ile296	Ile294	Ile294			Ile294		Ile299	Ile2
		His297												
					His300	His297			His300	His297				
					Val303	Val300			Val303	Val300			Val303	Val
TM VII														
							Tyr312	Tyr312			Tyr312	Tyr312		
						Trp318								Trp
			Ile316	Ile316	Ile325	Ile322	Ile316	Ile316		Ile322	Ile316	Ile316	Ile325	Ile3
		Gly325	Gly319	Gly319	Gly328	Gly325					Gly319	Gly319	Gly328	Gly
			Tyr320	Tyr320	Tyr329	Tyr326				Tyr326	Tyr320	Tyr320	Tyr329	Tyr

In addition to these conserved interactions, the models suggested additional receptor- and ligand-individual contact sites (Fig. 4). Fentanyl undergoes unique interactions with Gln127/124 and Trp136/133 in the cleft between TM II and III through its phenylethyl substituent (cMOR/rMOR). These interactions were absent in morphinan derived opioids. Buprenorphine displayed the most pronounced ligand-specific interaction pattern. Its 18-[(1S)-1-hydroxy-1,2,2-

trimethylpropyl]-6-methoxy substituent of the morphinan backbone specifically contacted Ser27/31/28, Gly28/30/27 and Trp29/32/29 in the N-terminal regions of cKOR, cMOR and rMOR. These interactions were not observed in the corresponding hKOR model. Buprenorphine also failed to interact with Tyr312 in the KOR models. This residue was previously implicated in k-receptor ligand stabilization and was involved in morphine and butorphanol binding [18]. Both buprenorphine and butorphanol faced Gly319/319/328/325 and Tyr320/320/329/326 in hKOR/cKOR/cMOR/rMOR with their common 17-(cyclopropylmethyl) moiety. Other differences included the absence of predicted lipophilic interactions between morphine and Ile299/296 in cMOR/rMOR, and between butorphanol and Ile294 in cKOR. All morphinan derivatives showed a unique interaction with His291 in cKOR, this residue has previously been implicated, together with Trp287, in ligand orientation and receptor activation [19]. All ligand contact sites are summarized in Table 1.

Predicted binding-pocket volumes also varied among ligands and receptors. Because it lacks substituents, morphine occupied the smallest predicted binding pockets, followed by butorphanol and buprenorphine. Again, buprenorphine exhibited the largest species-dependent differences, with a smaller pocket in cKOR compared to hKOR. By contrast, butorphanol occupied a larger pocket in cKOR than in the other receptor models (Table 2).

Table 2
Calculated ligand-binding pocket volumes. Values are the mean of three simulations and are reported in Å³ as mean ± SD values of n = 3 simulations.

Receptor	Fentanyl	Buprenorphine	Morphine	Butorphanol
hKOR		1,026.1 ± 88.5	768.6 ± 28.8	769.8 ± 63.6
cKOR		997.0 ± 31.9	731.1 ± 18.5	840.1 ± 20.0
cMOR	962.9 ± 148.1	1,069.0 ± 63.2	664.9 ± 113.5	810.1 ± 75.9
rMOR	1,097.0 ± 65.0	1,084.7 ± 25.3	666.5 ± 40.0	800.5 ± 43.9

A comparison of predicted and experimentally determined affinities (Fig. 5) showed a moderate correlation between predicted pK_i values and those obtained from radioligand binding (adjusted $R^2 = 0.669$). In contrast, the correlation between calculated free binding energies and experimental affinities was lower (adjusted $R^2 = 0.468$).

Species- and receptor-dependent differences in ERK1/2 signaling

Intrinsic activity was evaluated by agonist-stimulated ERK1/2 phosphorylation using maximum effective ligand concentrations. In HEK293 cells, this response is controlled by multiple redundant G protein-dependent and G protein-independent pathways [20], providing an integrative downstream readout not influenced by ligand biased signaling events [21]. Thus, maximum efficacy represents a measure for intrinsic activity in this system. Agonist-stimulated ERK1/2 phosphorylation revealed marked differences in intrinsic activity among receptor types and orthologs. Activation with saturating concentrations of the full reference agonists fentanyl (MOR) and U69,593 (KOR) resulted in 3- to 4-fold stimulation of ERK1/2 phosphorylation. This response was set to 100% maximum stimulation to calculate intrinsic activities of the opioid analgesics. By comparison, buprenorphine behaved as a moderate partial agonist at rMOR (43.08 ± 4.1%) and hKOR (50.88 ± 2.9%). It stimulated ERK1/2 phosphorylation to a much lower extent at cMOR (14.77 ± 4.7%) and cKOR (24.06 ± 4.8%), and these responses did not differ significantly from baseline. Morphine produced almost maximal ERK1/2 activation across all receptors tested, with responses of 77.11 ± 6.6% at rMOR, 69.99 ± 7.2% at cMOR, 83.87 ± 11.1% at cKOR and 72.97 ± 3.7% at hKOR. Butorphanol showed marked receptor dependence: ERK1/2 activation reached 105.58 ± 12.7% at cKOR and 78.54 ± 6.9% at hKOR, whereas it was lower at rMOR (45.91 ± 6.8%) and cMOR (24.44 ± 7.2%). Thus, the functional profile of butorphanol was particularly dependent on receptor type and orthologue (Fig. 6).

Discussion

The present study demonstrates ligand-specific differences in receptor affinity, selectivity, and intrinsic activity between canine opioid receptors and their rat MOR and human KOR reference counterparts. These findings are consistent with the concept that structural variation among receptor orthologues is associated with species-dependent drug pharmacology.

Buprenorphine provided the clearest example of this species dependence. It displayed very high affinity at all receptors, with the highest measured affinity at cMOR. In contrast, its intrinsic activity was significantly lower at canine receptors than at the corresponding reference receptors. These receptor-defined findings complement earlier work in dog brain membranes, in which buprenorphine also produced only little detectable G protein activation and, under some experimental conditions, even inhibited agonist-induced signaling in an antagonist-like manner [22]. This canine-specific profile of buprenorphine differs from that in other species [23]. In addition, variability in ligand profiles may arise from the presence of a mixed population of multiple opioid receptors, as well as from unidentified splice variants in the dog and individual receptor polymorphisms in the tissues used for characterization [3, 24–26].

The prototypical opioid analgesic morphine showed a canine specific increased MOR selectivity because of its significantly higher affinity at cMOR and lower affinity at cKOR compared to reference receptors. In addition, morphine showed almost full agonistic activity. However, the increased affinity could also contribute to the occurrence of adverse gastrointestinal effects and histamine release at therapeutic doses administered systematically [14, 27]. More sophisticated routes of morphine administration have therefore been developed in modern veterinary medicine [28].

Butorphanol exhibited the most pronounced canine-specific functional divergence. While its binding affinity was broadly similar across canine and human KOR and canine MOR, it acted as a full agonist at cKOR, in contrast to its effect at the human receptor. Combined with its low partial activity at cMOR, these receptor characteristics may influence the pharmacological actions of butorphanol in dogs [16, 17, 22].

The AlphaFold3-derived docking templates were validated against the human MOR and KOR experimental structures and provided a structural context for these pharmacodynamic differences. Consistent with the opioid message-address framework established for the δ-opioid receptor, all ligands occupied a conserved orthosteric binding pocket [29]. In addition, we identified divergent contacts at the N-terminus and TM VII. These sites were contacted by individual substituents of fentanyl and the morphinan derivatives in MOR and KOR [30–32]. However, the computational analysis did not predict species-specific contact sites associated with the enhanced affinity of morphine for canine MOR, its decreased affinity for KOR, or the increased affinity of butorphanol for both receptors. The computational analysis did not identify species-specific contacts that could explain the experimentally observed affinity differences of morphine and butorphanol, indicating that the current models may lack sufficient resolution to capture subtle effects of the few amino-acid substitutions distinguishing the receptor orthologues. This limitation was also reflected by the incomplete agreement between experimentally determined and predicted affinities. Neither the predicted affinity values nor free binding energies showed a one-to-one agreement with the experimental data. Continued improvement of these tools including consideration of N-terminal regions and extracellular loops as well as adaptation of ligand-specific high affinity states holds considerable promise for more accurate modeling of both ligand affinity and intrinsic activity [33]. One possible explanation is that our radioligand binding experiments measured ligand-receptor interactions under native conditions that encompassed an ensemble of different receptor conformations, whereas docking evaluates ligand interactions within one stable state of the receptor. Different conformational states and other experimental sources of variability may therefore help to improve the predicted interactions

Several limitations of this study should be noted. First, receptor pharmacology was investigated in a recombinant HEK293 cell system, which enables controlled, receptor-defined comparisons but does not fully replicate the cellular environment and signaling complexity of native canine tissues. Second, intrinsic activity was assessed using ERK1/2 phosphorylation as an integrated downstream signaling readout; while this approach captures multiple G protein-dependent and -independent pathways, ligand efficacy may differ depending on the signaling endpoint measured. Third, the study focused on MOR and KOR, and thus does not consider potential contributions from DOR, ORL1, receptor variants, or receptor interactions to opioid responses in vivo [4, 6, 34]. Finally, the computationally predicted ligand-receptor interactions remain hypothetical and require experimental validation through mutagenesis or other structure-function studies. Therefore, the ligand-specific pharmacological profiles described here should not be interpreted as direct predictions of clinical analgesic efficacy, which also depends on receptor distribution and density, pharmacokinetics, and the anatomical and functional organization of pain pathways.

Conclusion

Species-dependent variation in canine MOR and KOR sequences is associated with ligand- and receptor-dependent differences in opioid affinity and ERK1/2 signaling. Buprenorphine combined high affinity with reduced signaling at canine receptors, morphine retained near-maximal efficacy with enhanced canine MOR preference, and butorphanol showed pronounced KOR- and MOR-dependent differences in efficacy. Molecular docking identified conserved orthosteric contacts and ligand-specific interactions that may contribute to these effects. These findings provide receptor-level insights into species-dependent opioid pharmacology and support the integration of experimental and structural approaches in comparative pharmacology.

Methods

Cloning of canine opioid receptors

Cloning of the canine opioid receptors was complicated by the incomplete annotation of the reference canine genome sequence from a female Boxer (NW_003726046.1). The predicted canine OPRM1 sequence lacked a 39-bp region within exon 4 [35]. Using the homologous mouse sequence, this region was localized on canine chromosome 1 and primers were designed for RT-PCR cloning from a male Beagle hippocampal cDNA library (Zyagen, San Diego, CA, USA). Forward primers contained an N-terminal haemagglutinin (HA) tag. Primer sequences are provided in *table 3*. PCR products were subcloned into pcDNA3.1(+) expression vectors containing a geneticin-resistance gene. Constructs were verified by full insert Sanger sequencing and no polymorphisms in the Beagle sequences were detected compared to the predicted canis lupus familiaris OPRM1 and OPRK1 sequences from the annotation release 106 (XM_038653508.1; XM_038441075.1).

Cell lines and culture

Human embryonic kidney (HEK293) wild-type cells (DSMZ, Braunschweig, Germany) were transfected with jetPRIME reagent to stably express canine MOR (cMOR1), rat MOR (rMOR1), canine KOR (cKOR1) or human KOR (hKOR1). Stable clones were selected with 2,000 µg/mL G418 beginning 48 h after transfection. Receptor expression was confirmed by radioligand binding. The cell clones used in the experiments contained comparable amounts of high-affinity MOR (118.47 ± 18.6 and 84,61 ± 10.8 fmol/mg membrane protein for rMOR and cMOR, respectively) and KOR (127.76 ± 9.1 and 101.63 ± 25.3 fmol/mg membrane protein for hKOR and cKOR, respectively). These values resemble physiological levels in the brain [22].

Radioligand binding assays

Receptor affinity and selectivity were determined by radioligand binding to single receptor populations stably expressed in HEK293 cells under experimental conditions that favor the high-affinity, G protein-coupled receptor state.

Membrane preparation

Cells were harvested by centrifugation (300 × g, 4°C, 10 min) and homogenized in ice-cold buffer containing 5 mM Tris (pH 7.4), 1 mM EGTA and 1 mM DTT [20]. After low-speed centrifugation to remove unbroken cells and nuclei, membranes were collected at 20,000 × g for 30 min. Pellets were resuspended in TM buffer (50 mM Tris, pH 7.4, 5 mM $MgCl_2$) and used immediately.

Competition binding

Protein concentration was determined by the Lowry method [36]. Reactions contained 100 µg of membrane protein, 0.5 nM [^{3}H]naloxone and increasing concentrations of opioid ligands in a total volume of 0.2 ml TM Buffer, pH 7.4 [37]. Samples were incubated overnight at 4°C until equilibrium, followed by rapid filtration through glass-fibre filters treated with 1% PEG (Whatman GF/B). The filters were washed with ice-cold TM buffer, and radioactivity was quantified by scintillation counting. Specific binding was less than 10% of radioactivity added. Experiments were repeated three times, with duplicate determinations in each experiment. Specific binding was calculated by subtracting non-specific binding determined in the presence of 0.1 mM naloxone and was normalized to total binding. Competition curves were fitted using OriginPro. Naloxone K_d values were determined for each receptor from homologous displacement curves [38]. Inhibitory constants (K_i) were calculated from competition curves using the Cheng-Prusoff equation [39]. pK_i values are reported with the standard error (SE), and a pairwise statistical comparison was performed using a *t*-test.

Receptor docking studies

The AlphaFold3-derived docking templates were validated using experimentally determined structures (hMOR: 8ef6; hKOR; 9W49) [30, 40]. Using the MatchMaker tool in UCSF ChimeraX, the structures overlapped with a root-mean-square deviation (RMSD) of 0.805 Å across 265 pruned Cα pairs (1.463 Å across all 287 aligned pairs) for hMOR and RMSD of 1.180 Å across 198 pruned Cα pairs (2.899 Å across all 263 aligned pairs) for hKOR. Ligand-receptor interactions were modeled using Boltz-2 (default settings) [41–43] based on AlphaFold3 structural predictions [44]. Untagged receptor sequences were obtained from UniProt [45], and ligand structures were obtained from PubChem [46]. Three models were generated and analyzed for each receptor–ligand pair. Predicted affinity values were used for comparative analyses and converted to pK_i values for correlation analyses, which was performed based on all receptor-ligand combinations. Structural analysis was performed by using ChimeraX [47]. The ligand-binding pocket surface was calculated by generating a solvent-excluded molecular surface encompassing protein atoms within a 6.3 Å cutoff zone of the bound ligand. To isolate the continuous binding cavity and remove detached peripheral artifacts, surface rendering was restricted to the single largest contiguous surface patch. Amino-acid contacts were mapped and residues that interacted consistently across the three models for a given receptor-ligand pair were considered structurally relevant. Because these are computational predictions, the resulting contacts were interpreted qualitatively.

ERK1/2 phosphorylation assay

Intrinsic ligand activity was assessed in intact cells using agonist-stimulated ERK1/2 phosphorylation as an integrated downstream signaling readout. Cells were seeded at 200,000 cells/well, serum deprived for 30 min, equilibrated on ice and stimulated with maximum effective concentrations of opioid ligands determined in preliminary experiments (1 µM; 10 µM for morphine) for 6 min at 37°C. Reactions were terminated on ice and samples were processed for Western blotting [20].

Western blot analysis

Proteins were separated by SDS-PAGE on 10% polyacrylamide gels and transferred to PVDF membranes. The membranes were blocked and probed with anti-phospho-ERK1/2 antibodies. Total protein staining was used for normalization [48]. Immunoreactive bands were quantified using Image Lab software, normalized and expressed as a percentage of maximal stimulation by a full agonist (1 µM fentanyl for MOR and 1 µM U69,593 for KOR). Results are therefore reported as relative efficacy for ERK1/2 phosphorylation. Data are presented as the mean with SE. After normality was confirmed using the Shapiro-Wilk test, statistical comparisons were performed using one-way ANOVA with post-hoc Tukey.

Declarations

Competing Interests

The authors declare no competing interests.

Ethics Statement

No live animals or human participants were used in this study. All experiments were performed using established recombinant receptor constructs expressed in HEK293 cells and in vitro biochemical and cellular assays, complemented by computational structural modeling. Consequently, no animal or human ethics approval was required.

Use of AI

The Nature Research Assistant was used to improve the manuscript.

Funding

This work was supported by a grant from the VetResearch program of the Faculty of Veterinary Medicine, Ludwig-Maximilians-Universität München, awarded to Christian Zenner.

Author Contribution

SKA and CZ: Cloned the canine OPRM1 and OPRK1 and performed the initial pharmacological characterization.EKG: Designed the study, performed, analyzed, and interpreted all experiments; performed the statistical analysis and data visualization and wrote the manuscript.HA: Designed the study, wrote and edited the manuscript.All authors have read and agreed to the published version of the manuscript.

Acknowledgement

The authors thank Moritz Lattner for expert technical assistance.

Data Availability

The datasets generated and/or analyzed during the current study are available under the following NCBI accession links: NW_003726046.1; https://www.ncbi.nlm.nih.gov/nuccore/NW_003726046.1?report=genbankKP676947.1; https://www.ncbi.nlm.nih.gov/nuccore/KP676947.1KP676946.1; https://www.ncbi.nlm.nih.gov/nuccore/KP676946.1

References

1. Bradbrook, C. A. & Clark, L. State of the art analgesia- recent developments in pharmacological approaches to acute pain management in dogs and cats. Part 1. *Vet. J.* **238**, 76–82 (2018).
2. Toutain, P. L., Ferran, A. & Bousquet-Mélou, A. *Species differences in pharmacokinetics and pharmacodynamics*. *Handb. Exp. Pharmacol.*, (199): pp. 19–48. (2010).
3. Kongara, K. Pharmacogenetics of opioid analgesics in dogs. *J. Vet. Pharmacol. Ther.* **41** (2), 195–204 (2018).
4. Khalefa, B. I. et al. Relative contributions of peripheral versus supraspinal or spinal opioid receptors to the antinociception of systemic opioids. *Eur. J. Pain*. **16** (5), 690–705 (2012).
5. Gallantine, E. L. & Meert, T. F. Antinociceptive and adverse effects of mu- and kappa-opioid receptor agonists: a comparison of morphine and U50488-H. *Basic. Clin. Pharmacol. Toxicol.* **103** (5), 419–427 (2008).
6. Rivière, P. J. Peripheral kappa-opioid agonists for visceral pain. *Br. J. Pharmacol.* **141** (8), 1331–1334 (2004).
7. Chu, S., Chung, P. & Kieffer, B. L. Delta opioid receptors in brain function and diseases. *Pharmacol. Ther.* **140** (1), 112–120 (2013).
8. Law, P. Y., Wong, Y. H. & Loh, H. H. Molecular mechanisms and regulation of opioid receptor signaling. *Annu. Rev. Pharmacol. Toxicol.* **40**, 389–430 (2000).
9. Zhang, L., Loh, H. H. & Law, P. Y. A novel noncanonical signaling pathway for the μ-opioid receptor. *Mol. Pharmacol.* **84** (6), 844–853 (2013).
10. Mann, A. et al. Agonist-induced phosphorylation bar code and differential post-activation signaling of the delta opioid receptor revealed by phosphosite-specific antibodies. *Sci. Rep.* **10** (1), 8585 (2020).
11. Koch, T. et al. Receptor endocytosis counteracts the development of opioid tolerance. *Mol. Pharmacol.* **67** (1), 280–287 (2005).
12. De Neve, J. et al. Comprehensive overview of biased pharmacology at the opioid receptors: biased ligands and bias factors. *RSC Med. Chem.* **12** (6), 828–870 (2021).
13. Martinez, S. A. et al. The safety and effectiveness of a long-acting transdermal fentanyl solution compared with oxymorphone for the control of postoperative pain in dogs: a randomized, multicentered clinical study. *J. Vet. Pharmacol. Ther.* **37** (4), 394–405 (2014).
14. Guedes, A. G., Rudé, E. P. & Rider, M. A. Evaluation of histamine release during constant rate infusion of morphine in dogs. *Vet. Anaesth. Analg*. **33** (1), 28–35 (2006).
15. Robinson, K. J., Jones, R. S. & Cripps, P. J. Effects of medetomidine and buprenorphine administered for sedation in dogs. *J. Small Anim. Pract.* **42** (9), 444–447 (2001).
16. Hayashi, K. et al. Comparison of sedative effects induced by medetomidine, medetomidine-midazolam and medetomidine-butorphanol in dogs. *J. Vet. Med. Sci.* **56** (5), 951–956 (1994).
17. Sawyer, D. C. et al. Dose response to butorphanol administered subcutaneously to increase visceral nociceptive threshold in dogs. *Am. J. Vet. Res.* **52** (11), 1826–1830 (1991).
18. Lavecchia, A. et al. Modeling of kappa-opioid receptor/agonists interactions using pharmacophore-based and docking simulations. *J. Med. Chem.* **43** (11), 2124–2134 (2000).
19. Saleh, A. H. et al. Deciphering the molecular basis of the kappa opioid receptor selectivity: A Molecular Dynamics study. *J. Mol. Graph Model.* **106**, 107940 (2021).
20. Eisinger, D. A. & Ammer, H. Epidermal growth factor treatment switches δ-opioid receptor-stimulated extracellular signal-regulated kinases 1 and 2 signaling from an epidermal growth factor to an insulin-like growth factor-1 receptor-dependent mechanism. *Mol. Pharmacol.* **79** (2), 326–335 (2011).
21. Gillis, A., Sreenivasan, V. & Christie, M. J. Intrinsic Efficacy of Opioid Ligands and Its Importance for Apparent Bias, Operational Analysis, and Therapeutic Window. *Mol. Pharmacol.* **98** (4), 410–424 (2020).
22. Lester, P. A. & Traynor, J. R. *Comparison of the in vitro efficacy of mu, delta, kappa and ORL1 receptor agonists and non-selective opioid agonists in dog brain membranes*. *Brain Res.*, 1073–1074 : pp. 290–6. (2006).

23. Harmar, A. J. et al. IUPHAR-DB: the IUPHAR database of G protein-coupled receptors and ion channels. *Nucleic Acids Res.* **37** (Database issue), D680–D685 (2009).
24. Abrimian, A., Kraft, T. & Pan, Y. X. *Endogenous Opioid Peptides and Alternatively Spliced Mu Opioid Receptor Seven Transmembrane Carboxyl-Terminal Variants*. *Int. J. Mol. Sci.*, **22**(7). (2021).
25. Befort, K. et al. A single nucleotide polymorphic mutation in the human mu-opioid receptor severely impairs receptor signaling. *J. Biol. Chem.* **276** (5), 3130–3137 (2001).
26. Selley, D. E., Liu, Q. & Childers, S. R. Signal transduction correlates of mu opioid agonist intrinsic efficacy: receptor-stimulated [35S]GTP gamma S binding in mMOR-CHO cells and rat thalamus. *J. Pharmacol. Exp. Ther.* **285** (2), 496–505 (1998).
27. Guedes, A. G. et al. Pharmacokinetics and physiological effects of two intravenous infusion rates of morphine in conscious dogs. *J. Vet. Pharmacol. Ther.* **30** (3), 224–233 (2007).
28. Morgaz, J. et al. Preperitoneal ropivacaine infusion versus epidural ropivacaine-morphine for postoperative analgesia in dogs undergoing ovariohysterectomy: a randomized clinical trial. *Vet. Anaesth. Analg*. **48** (6), 935–942 (2021).
29. Granier, S. et al. Structure of the δ-opioid receptor bound to naltrindole. *Nature* **485** (7398), 400–404 (2012).
30. Zhuang, Y. et al. Molecular recognition of morphine and fentanyl by the human μ-opioid receptor. *Cell* **185** (23), 4361–4375e19 (2022).
31. Gomes, A. A. S. & Giraldo, J. Structural Determinants of Buprenorphine Partial Agonism at the μ-Opioid Receptor. *J. Chem. Inf. Model.* **65** (10), 5071–5085 (2025).
32. Ji, J. et al. Molecular Interaction Between Butorphanol and κ-Opioid Receptor. *Anesth. Analg*. **131** (3), 935–942 (2020).
33. Heydenreich, F. M. et al. Molecular determinants of ligand efficacy and potency in GPCR signaling. *Science* **382** (6677), eadh1859 (2023).
34. Vieira, C. M. P. et al. Pain polymorphisms and opioids: An evidence based review. *Mol. Med. Rep.* **19** (3), 1423–1434 (2019).
35. Sayers, E. W. et al. Database resources of the National Center for Biotechnology Information in 2025. *Nucleic Acids Res.* **53** (D1), D20–d29 (2025).
36. Lowry, O. H. et al. Protein measurement with the Folin phenol reagent. *J. Biol. Chem.* **193** (1), 265–275 (1951).
37. Flanagan, C. A. GPCR-radioligand binding assays. *Methods Cell. Biol.* **132**, 191–215 (2016).
38. DeBlasi, A., O'Reilly, K. & Motulsky, H. J. Calculating receptor number from binding experiments using same compound as radioligand and competitor. *Trends Pharmacol. Sci.* **10** (6), 227–229 (1989).
39. Cheng, Y. & Prusoff, W. H. Relationship between the inhibition constant (K1) and the concentration of inhibitor which causes 50 per cent inhibition (I50) of an enzymatic reaction. *Biochem. Pharmacol.* **22** (23), 3099–3108 (1973).
40. Suno-Ikeda, C. et al. Structural and dynamic insights into the biased signaling mechanism of the human kappa opioid receptor. *Nat. Commun.* **16** (1), 9392 (2025).
41. Amani, K. *Neurosnap: An online platform for computational biology and chemistry*. [cited 2025; (2022). Available from: https://neurosnap.ai/
42. Mirdita, M. et al. ColabFold: making protein folding accessible to all. *Nat. Methods*. **19** (6), 679–682 (2022).
43. Passaro, S. et al. *Boltz-2: Towards Accurate and Efficient Binding Affinity Prediction.* bioRxiv, (2025).
44. Abramson, J. et al. Accurate structure prediction of biomolecular interactions with AlphaFold 3. *Nature* **630** (8016), 493–500 (2024).
45. Consortium, T. U. UniProt: the Universal Protein Knowledgebase in 2025. *Nucleic Acids Res.* **53** (D1), D609–D617 (2024).
46. Kim, S. et al. PubChem 2025 update. *Nucleic Acids Res.* **53** (D1), D1516–D1525 (2024).
47. Meng, E. C. et al. UCSF ChimeraX: Tools for structure building and analysis. *Protein Sci.* **32** (11), e4792 (2023).
48. Pillai-Kastoori, L., Schutz-Geschwender, A. R. & Harford, J. A. A systematic approach to quantitative Western blot analysis. *Anal. Biochem.* **593**, 113608 (2020).
49. Omasits, U. et al. Protter: interactive protein feature visualization and integration with experimental proteomic data. *Bioinformatics* **30** (6), 884–886 (2014).

Figures

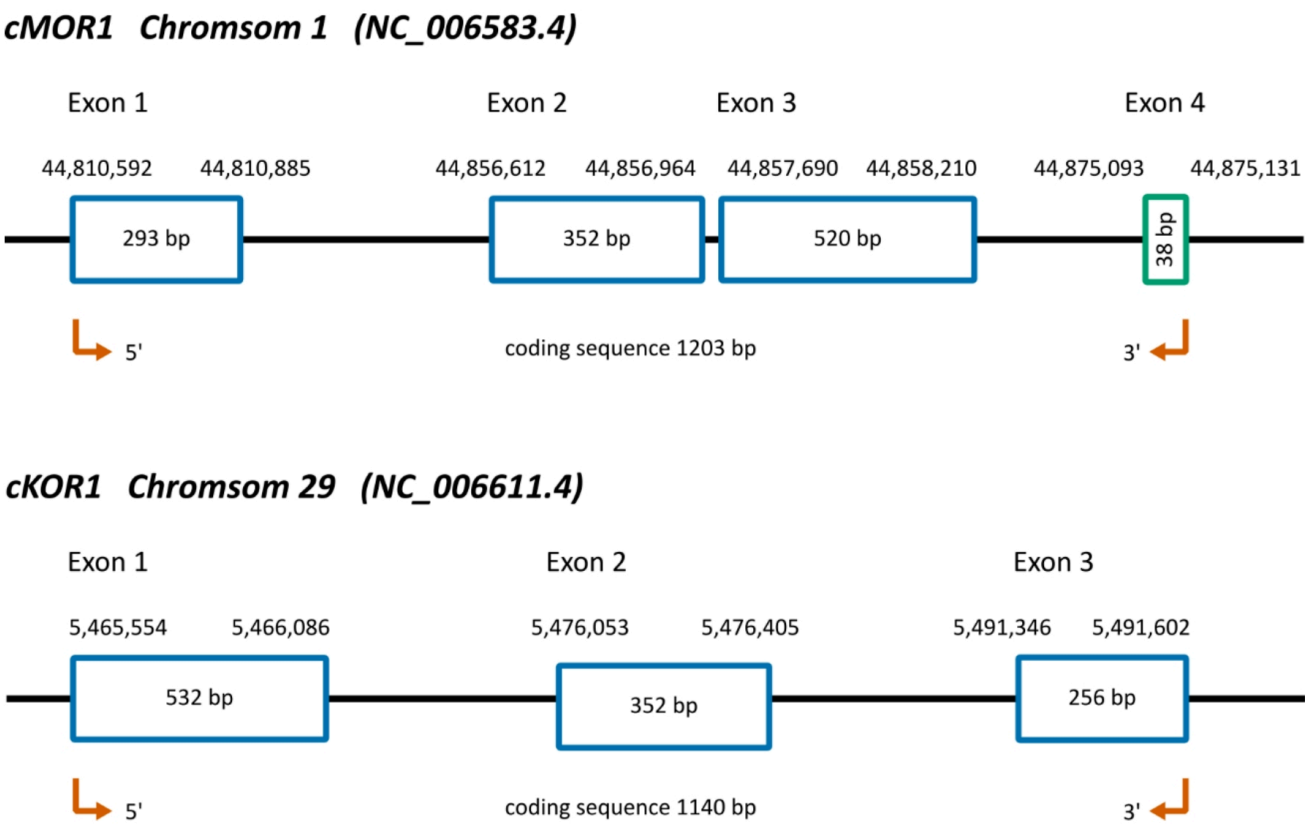


Figure 1

Genomic organization of canine opioid receptors. Chromosome 1 encodes cMOR1. The missing exon 4 sequence in the predicted reference sequence was localized with the aid of the mouse genome and incorporated into the cloned sequence. Chromosome 29 encodes cKOR1.

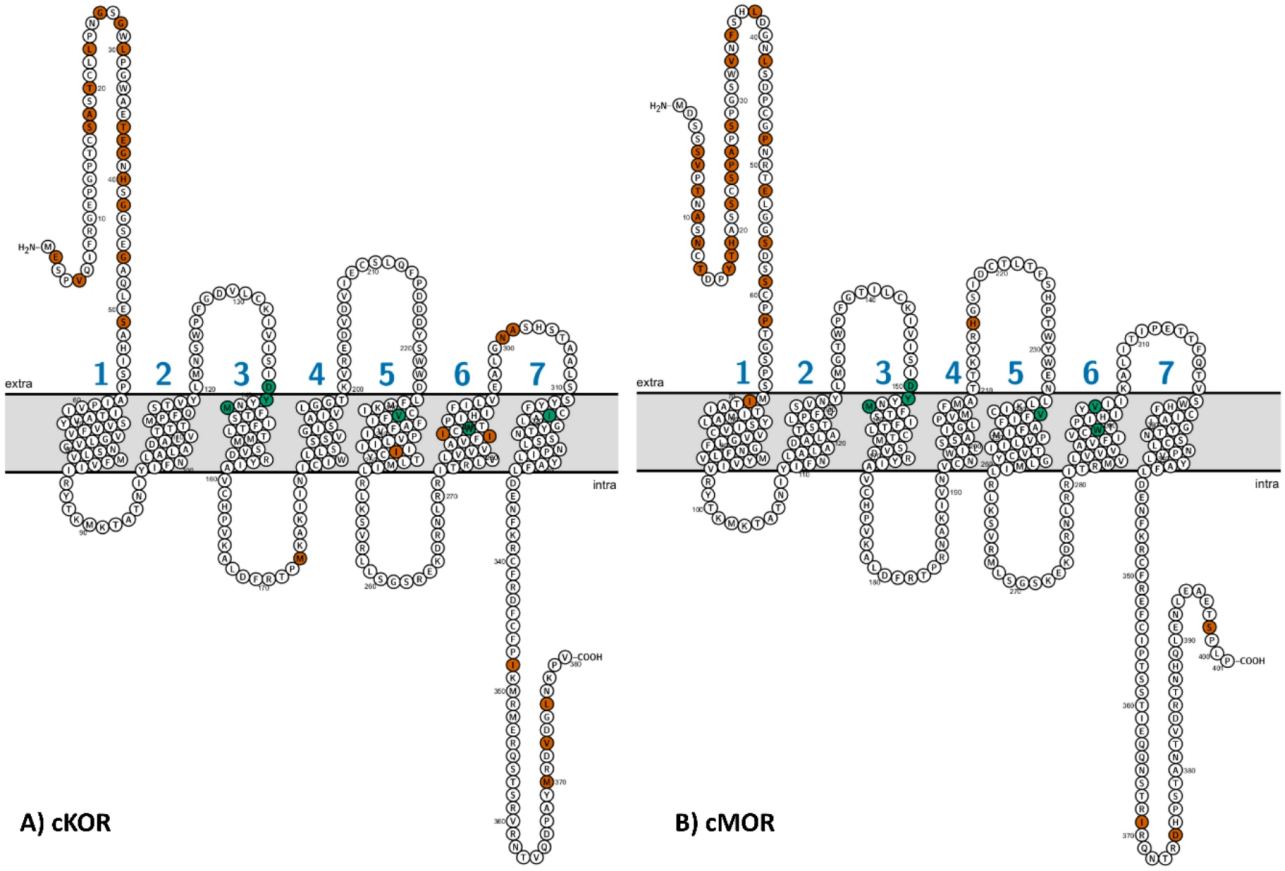


Figure 2

Snake plots of canine MOR (A) and KOR (B). Transmembrane domains are numbered 1–7. Amino-acid differences between canine receptors and the corresponding human or rat reference receptors are highlighted in red. Conserved residues implicated in ligand binding are indicated in green. The diagrams were generated with Protter [49].

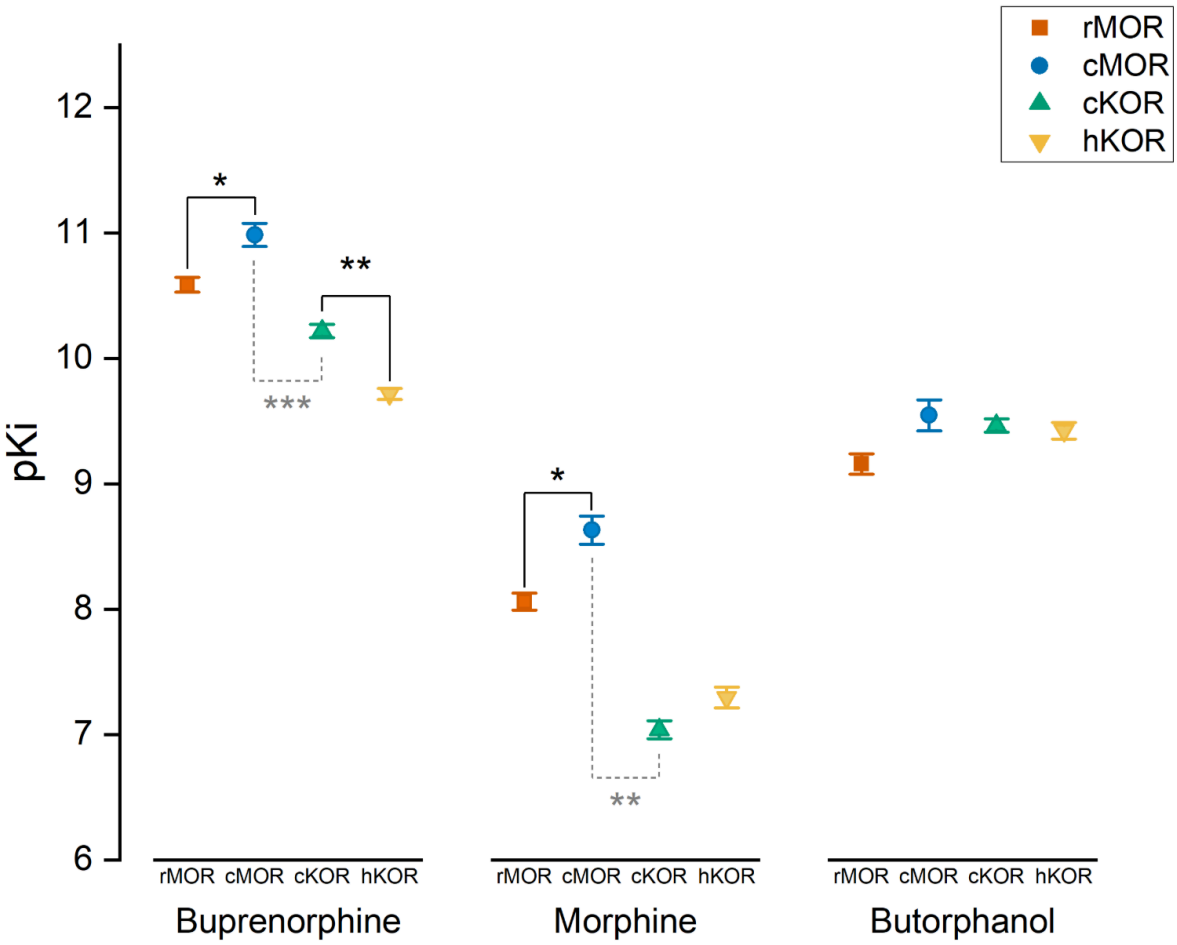


Figure 3

Binding affinities of opioid ligands at canine and reference opioid receptors. Data are shown as pK_i values with standard error (SE). Three experiments were performed in duplicates (n = 3), *$p < 0.05$, **$p < 0.01$, ***$p < 0.001$.

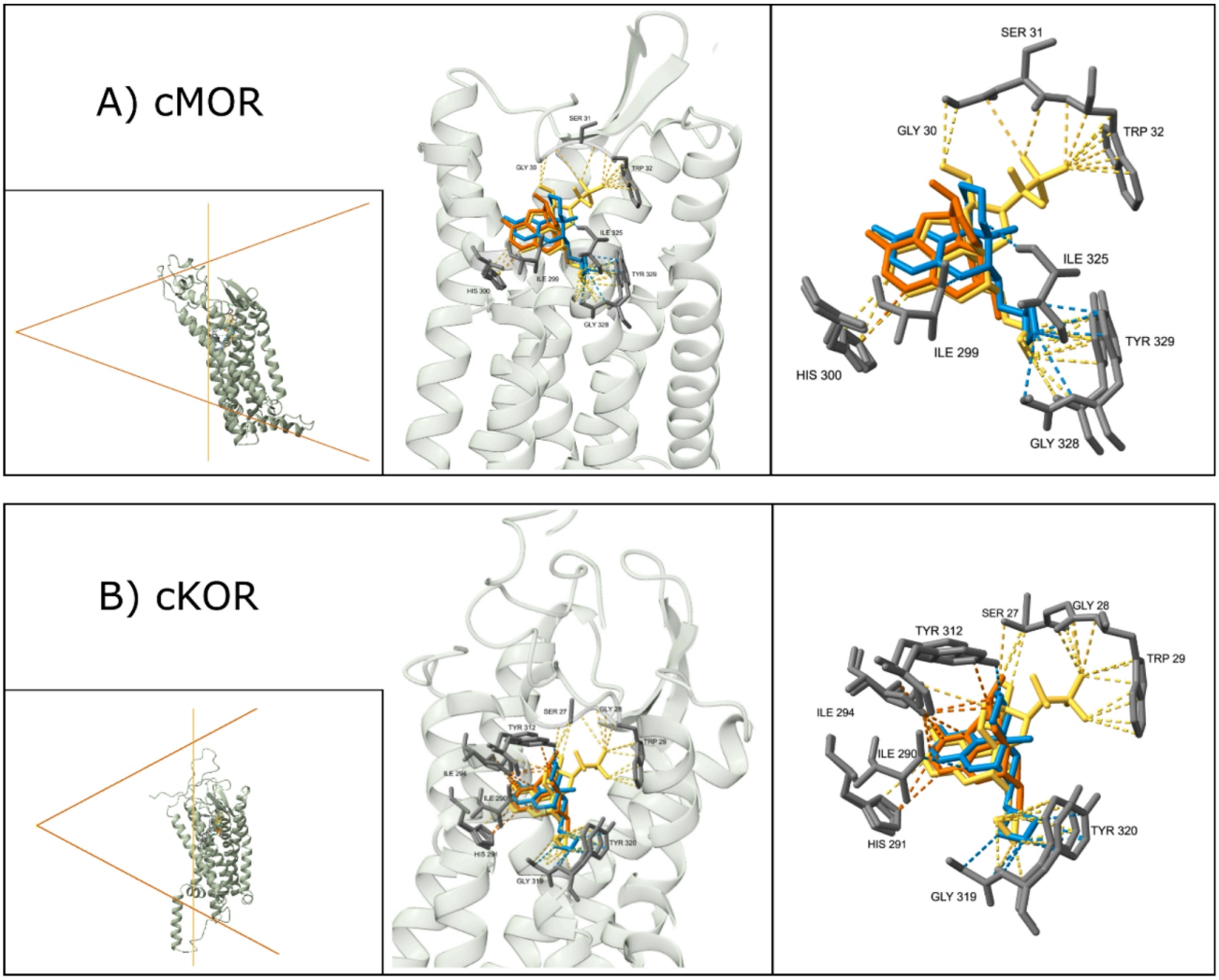


Figure 4

Representative ligand–receptor docking models. Receptor backbones are shown in grey, together with amino acid residues that showed ligand-specific interactions across the three models for each receptor-ligand combination. Buprenorphine, butorphanol and morphine are distinguished by color; yellow: buprenorphine, red: morphine, blue: butorphanol. Conserved contacts are summarized in *figure* 2 and *table*1.

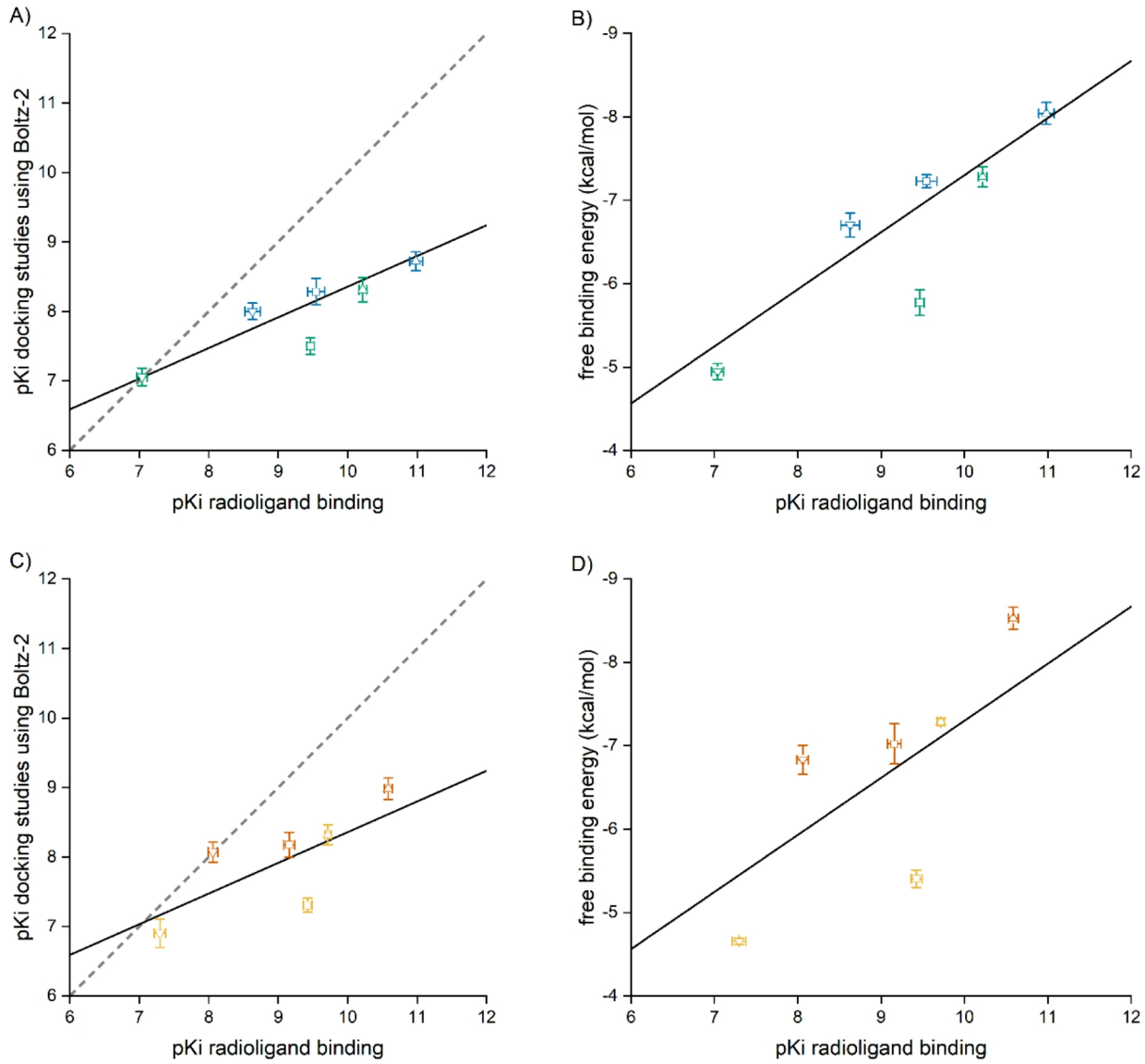


Figure 5

Comparison of experimentally determined and predicted ligand affinities. Experimental pK_i values are plotted against predicted pK_i values (A,C) and calculated free binding energies (B,D). Error bars indicate SE. The dashed line represents x = y and the solid lines represent linear fits. Panels A and B show cKOR1 (green) and cMOR1 (blue); panels C and D show hKOR1 (yellow) and rMOR1 (red).

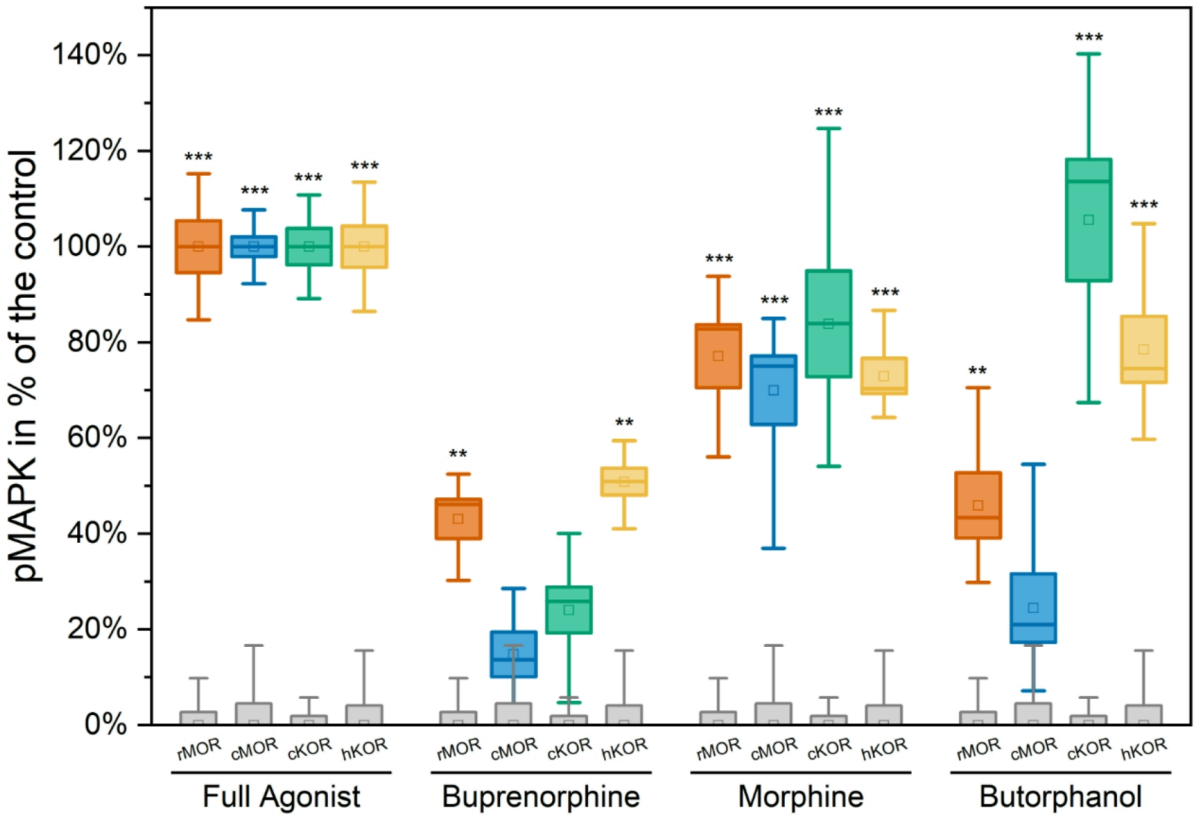


Figure 6

Opioid-induced ERK1/2 phosphorylation at canine and reference opioid receptors. Responses are expressed as a percentage of maximal stimulation by fentanyl at MOR or U69,593 at KOR. The box plot shows the median with the box representing the standard error (SE) and the whiskers indicating the 5th and 95th percentiles, of n = 6 experiments. For each receptor, basal pERK1/2 activity is shown in grey at the lower edge of the figure. Significant differences to basal activity are indicated as *$p < 0.05$, **$p < 0.01$, ***$p < 0.001$.

Supplementary Files

This is a list of supplementary files associated with this preprint. Click to download.

- SciRepGerdesSupplementaryMaterials.docx